A compact neutron spectrometer for characterizing inertial confinement fusion implosions at OMEGA and the NIF

A. B. Zylstra, M. Gatu Johnson, J. A. Frenje, F. H. Séguin, H. G. Rinderknecht, M. J. Rosenberg, H. W. Sio, C. K. Li, R. D. Petrasso, M. McCluskey, D. Mastrosimone, V. Yu. Glebov, C. Forrest, C. Stoeckl, and T. C. Sangster

Citation: Review of Scientific Instruments **85**, 063502 (2014); doi: 10.1063/1.4880203
View online: http://dx.doi.org/10.1063/1.4880203
View Table of Contents: http://scitation.aip.org/content/aip/journal/rsi/85/6?ver=pdfcov
Published by the AIP Publishing

A compact neutron spectrometer for characterizing inertial confinement fusion implosions at OMEGA and the NIF

A. B. Zylstra,[1,a)] M. Gatu Johnson,[1] J. A. Frenje,[1] F. H. Séguin,[1] H. G. Rinderknecht,[1] M. J. Rosenberg,[1] H. W. Sio,[1] C. K. Li,[1] R. D. Petrasso,[1] M. McCluskey,[2] D. Mastrosimone,[2] V. Yu. Glebov,[2] C. Forrest,[2] C. Stoeckl,[2] and T. C. Sangster[2]
[1]*Plasma Science and Fusion Center, Massachusetts Institute of Technology, Cambridge, Massachusetts 02139, USA*
[2]*Laboratory for Laser Energetics, University of Rochester, Rochester, New York 14623, USA*

(Received 1 April 2014; accepted 16 May 2014; published online 4 June 2014)

A compact spectrometer for measurements of the primary deuterium-tritium neutron spectrum has been designed and implemented on the OMEGA laser facility [T. Boehly *et al.*, Opt. Commun. **133**, 495 (1997)]. This instrument uses the recoil spectrometry technique, where neutrons produced in an implosion elastically scatter protons in a plastic foil, which are subsequently detected by a proton spectrometer. This diagnostic is currently capable of measuring the yield to ~±10% accuracy, and mean neutron energy to ~±50 keV precision. As these compact spectrometers can be readily placed at several locations around an implosion, effects of residual fuel bulk flows during burn can be measured. Future improvements to reduce the neutron energy uncertainty to ±15−20 keV are discussed, which will enable measurements of fuel velocities to an accuracy of ~±25−40 km/s. © *2014 AIP Publishing LLC*. [http://dx.doi.org/10.1063/1.4880203]

I. INTRODUCTION

In inertial confinement fusion (ICF) implosions at OMEGA[1] and the National Ignition Facility (NIF),[2] a spherical shell of fuel is ablatively driven inwards at implosion velocities of ~370 km/s. This imploding shell is decelerated by the central low-density high-temperature "hot spot," which reaches pressures of ~300 GBar in ideal fusion target designs.[3–5] Efficient conversion of this implosion kinetic energy into hot spot thermal energy is essential for achieving ignition. Any residual fuel kinetic energy at peak compression represents a deficit in thermal energy, which will significantly reduce the fusion burn rate in the hot spot and can cause the implosion to fail to ignite.

Neutron spectroscopy has been identified as a promising technique for diagnosing residual kinetic energy in the fuel,[6,7] in addition to well-established measurements of areal density, total yield, and ion temperature.[8] Neutron spectroscopy techniques in-use at the OMEGA and NIF facilities include neutron time-of-flight (nTOF),[9,10] nuclear activation,[11,12] and recoil spectroscopy.[13–18]

The primary signature of residual kinetic energy would be a Doppler shift of the neutron spectrum; for relevant conditions the Doppler shift is approximately linear through relativistic kinematics (see Appendix B). This is shown in Fig. 1 for neutrons produced via the deuterium-tritium (DT) fusion reaction, expressed as

$$\mathrm{D} + \mathrm{T} \rightarrow \alpha + \mathrm{n}(14.03\ \mathrm{MeV}), \tag{1}$$

where the neutron birth energy is 14.03 MeV at zero temperature and is upshifted for finite temperatures.[19] The spectral Doppler shifts will be of order a few tens of keV for DT neutrons if the residual velocity is a significant fraction of the 370 km/s implosion velocity at NIF. The magnitude of observed energy shift depends on the direction of bulk flow velocity ($\vec{v_b}$) relative to the detector ($\hat{r}$):

$$v = \vec{v_b} \cdot \hat{r} = v_b \cos\theta, \tag{2}$$

which necessitates that spectrometers be placed in at least three quasi-orthogonal lines of sight to fully diagnose residual kinetic energy through Doppler shifts of the mean neutron energy. As shown by Eq. (2), a single detector is only sensitive to the velocity collinear with the line of sight. In recent experiments at the NIF velocities (Doppler shifts) up to ~200 km/s (100 keV) have been observed.[6] The ignition point design[4] accelerates ~0.17 mg of DT fuel to an implosion velocity ~370 km/s corresponding to 11 kJ of kinetic energy. Diagnosing residual kinetic energy of 250(1000)J, representing approximately 2.5(10)% of the total kinetic energy, would correspond to bulk velocities of ~50(100) km/s or neutron Doppler shifts of ~25(50) keV. For NIF, this suggests a desired measurement accuracy of ±50 keV or more ideally ±20 keV.

This paper describes a new uniquely compact neutron spectrometer based on the recoil technique for diagnosing ICF implosions. A CH foil is used to generate recoil protons, which are detected with a Wedge Range Filter proton spectrometer.[20,21] This design is advantageous for measurements of the residual kinetic energy, since many spectrometers could easily be fielded around the implosion. The proton spectrometer is unshielded (exposed directly to the primary neutron flux), allowing S/B of order 1 for the primary neutron peak.[13] This is in contrast to the "magnetic recoil spectrometer" (MRS) system using dipole magnetic dispersion,[13–15] which improves the S/B significantly since the charged particles can be bent around shielding to reduce background.[15,22] However, the MRS is a large investment, and only one has

a)Electronic mail: zylstra@mit.edu

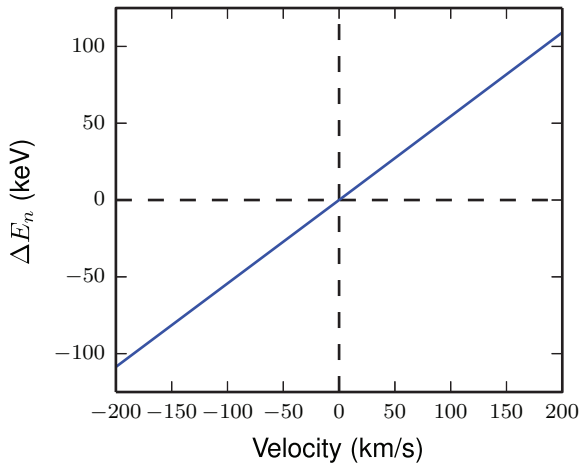

FIG. 1. Neutron Doppler shift (ΔE_n) versus fuel bulk velocity in the direction of the spectrometer.

been built on each facility (OMEGA and the NIF). Recoil spectrometers have also been developed at other facilities using telescope systems.[23–26] We note that we have also developed a related concept[42] for a compact spectrometer designed for lower-energy neutrons (∼1 to 5 MeV).

This paper is organized as follows: Section II describes the concept and design of the instrument, Sec. III presents response calculations for data analysis, Sec. IV reports data from the first use of this system on OMEGA, applications of this diagnostic to ICF physics are discussed in Sec. V, and the paper is concluded in Sec. VI.

II. SPECTROMETER DESIGN

The conceptual design of the instrument is shown in Fig. 2. A small fraction of the neutrons emitted from the implosion hit a foil, in this case CH_2, and elastically scatter protons, some of which are detected by a proton spectrometer (WRF+CR-39).

The energy of a recoil proton is directly related to the incident neutron energy through the scattering angle, as described by

$$E_r = E_n \cos^2\theta, \tag{3}$$

where E_r and E_n are the recoil and neutron energies, respectively, and θ is the scattering angle. Given the geometry, the detector efficiency can be written semi-analytically,[15] but the characterization of the energy response will depend on numerical modeling of the charged-particle stopping powers in the foil[27] and also on the WRF response itself. Monte Carlo simulations are therefore used to model the instrument response function (IRF).

In this work, two types of proton spectrometers are used: an aluminum or "Al" wedge which varies in thickness from ∼140 to 2000 μm and is approximately 2 cm square in lateral dimensions, and a ceramic (alumina) narrow-band "NB" wedge which varies in thickness from ∼100 to 800 μm with lateral dimensions of ∼1 × 4 cm. For the NB wedges, the dispersion direction is the longer axis, and two wedges can be run simultaneously and adjacently within a single package. Both designs were tested; the NB WRFs have a higher efficiency at the cost of less energy resolution. Positioned behind the wedge material is a piece of CR-39 solid-state nuclear track detector,[28–30] which records the location and energy of the protons that have penetrated the wedge. From the CR-39 track distribution, a proton energy spectrum is inferred.[20,21] Each wedge is individually calibrated on an electrostatic accelerator fusion product source.[31]

The key parameters for the instrument are the foil dimensions (diameter and thickness), foil distance from the implosion, detector lateral dimensions, and foil-to-detector distance. It is important to note that there is a direct trade-off between energy resolution and detection efficiency.[32] To find the optimal design for the instrument, series of simulations were conducted in which the key parameters were varied until maximum efficiency for a specified energy resolution was found. This modeling was also constrained by the geometric limits of Ten-Inch Manipulator (TIM) diagnostics on the OMEGA facility, and with the requirement that S/B must be $\gtrsim$0.5 for OMEGA experiments with $Y_n = 10^{12}-10^{13}$. For these conditions, the optimal design is a foil radius of ∼1 cm, with the foil positioned ∼4 cm from the implosion, and a foil-detector distance of ∼25 cm. Additionally, the existing WRF designs[20,21] were found to perform adequately, and are thus used in this design.

Depending on application and experimental goals, the foil thickness can be changed easily, affecting the number of counts recorded, S/B, and resolution. This is shown in Fig. 3 for both types of WRF (Al and NB), where these three quantities are plotted for foil thicknesses up to 200 μm. For very thin foils, the instrument resolution (FWHM) is dominated by "geometrical broadening," where the proton spectrometer

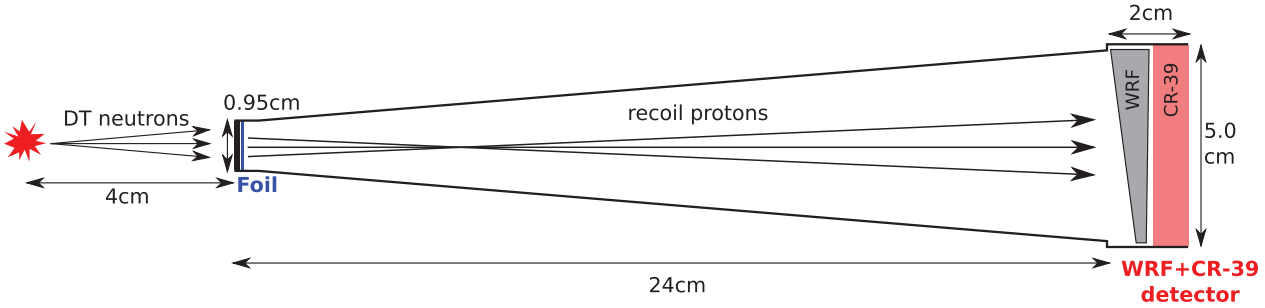

FIG. 2. Conceptual spectrometer design. A small fraction of the DT neutrons generated in the implosion (at left) hit a CH_2 foil, and elastically scatter protons. Forward-scattered protons are detected by a wedge-range-filter (WRF) and CR-39 package (far right). From the measured recoil-proton spectrum, the spectrum of the emitted neutrons can be inferred. The dimensions shown are for an optimal design at OMEGA-relevant conditions.

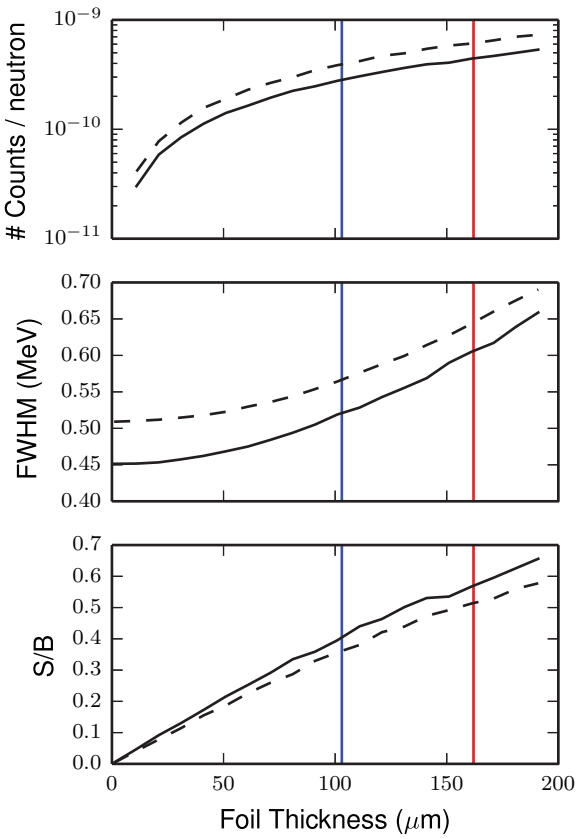

FIG. 3. Performance of the optimal nWRF design as a function of foil thickness. (a) Number of counts recorded per neutron generated (efficiency). (b) Resolution, shown as FWHM. For thin foils, the resolution is dominated by geometric broadening and the WRF response. (c) Signal to background (S/B). In all plots, solid curves correspond to Al WRFs and dashed curves correspond to Narrow-Band (NB) WRFs. Foils used in the experiments (Sec. IV) are shown by blue (103 μm) and red (162 μm) vertical lines.

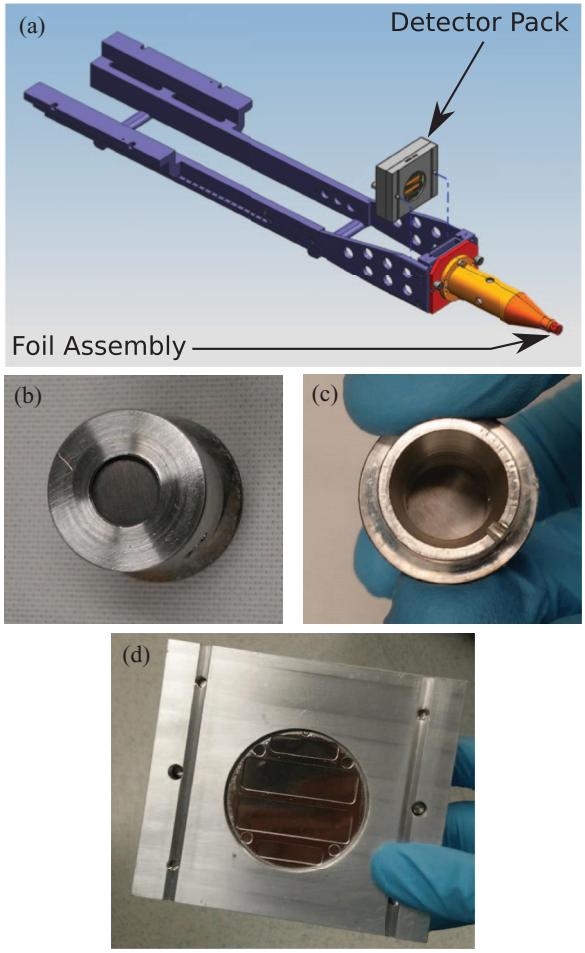

FIG. 4. (a) 3D CAD model of the instrument. The proton spectrometer is housed in the gray box, which is attached at the rear of a conical nose assembly. The foil assembly is at the tip in the lower right. The rail structures in the upper left interface with the facility instrument manipulator. (b-c) Photos of a sample foil assembly, viewed from and towards TCC, respectively. (d) Detector pack. A NB WRF proton spectrometer is held at the center.

sees a range of recoil angles due to the lateral spatial extent of the foil (see Fig. 2 and Eq. (3)). Since the signal and primary source of background (direct neutron interaction, see Appendix D) scale linearly with primary yield, S/B depends only on the instrument configuration.

The final dimensions are shown in Fig. 2. The engineering design is based on a x-ray camera already in use on the OMEGA facility. A Computer-aided Design (CAD) drawing of the instrument is shown in Fig. 4. The WRF proton spectrometer is held in a detector pack, while the foil is assembled as a "nose cone" at the front of the instrument. A 1 mm thick Ta blast filter is placed between Target Chamber Center (TCC) and the foil. Images of the foil assembly and detector pack are shown in Figs. 4(b)–4(d). The foil and detector can be changed between shots. For different experimental conditions (for example, either lower or higher yields) different optimal designs can be used.

III. INSTRUMENT RESPONSE FUNCTION MODELING

A Monte Carlo code is used to simulate the n-p scattering in the foil, ranging of the recoil protons in the foil, transport of the recoil protons through the diagnostic geometry to the WRF detector, and the response of the WRF detector to protons. For a given neutron energy, recoil protons are tracked and the proton spectrometer response is simulated, such that an apparent proton spectrum on the detector is calculated for a given neutron energy. This is shown in Fig. 5 for 14.05 MeV neutrons incident on two foils (103 and 162 μm thick) and for both types of WRF used (Al and NB).

The curves in Fig. 5 are normalized per neutron produced, and the apparent proton yield is calculated as a 4π equivalent yield.[33] Using the 162 μm foil results in more proton signal due to the higher areal number density of the thicker foil. Similarly, the thicker foil generates a lower average proton energy, since the emerging protons are on average downshifted more in the thicker foil. The slight differences between WRF types arise from subtle differences in the WRF geometry, which affects the scattering angles for protons used in the analysis.

To calculate an IRF, a series of calculations are performed for the neutron energy range of interest, with a proton spectrum calculated for each neutron energy, thus generating a response matrix. In the data analysis, we convolve a trial Gaussian neutron spectrum with the IRF matrix to calculate a modeled proton spectrum. Thus, we can forward fit the data using the IRF.

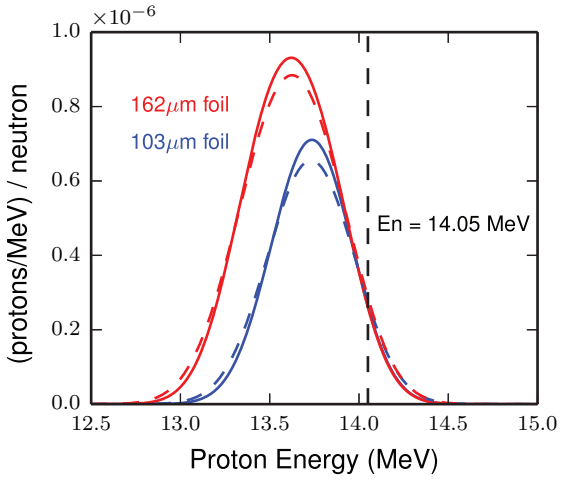

FIG. 5. Proton spectrum for 14.05 MeV monoenergetic neutrons. Shown are calculations for 103 μm (blue) and 162 μm (red) thick foils. Solid spectra are for Al WRFs, and dashed spectra are for NB WRFs.

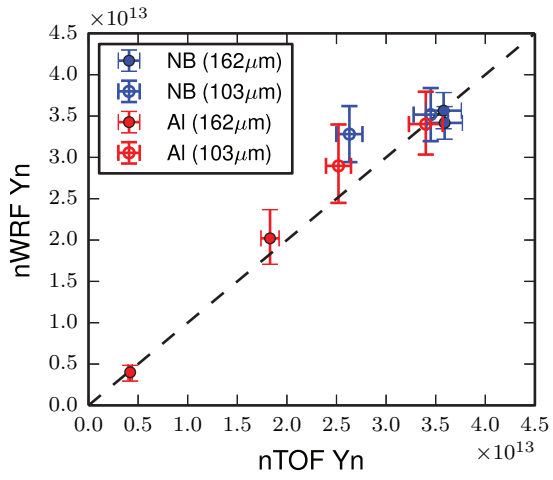

FIG. 7. Neutron yields measured by the nWRF versus standard nTOF neutron yield, for both Al and NB wedges used with either a 103 μm or 162 μm foil.

IV. OMEGA RESULTS

A series of eight implosions were conducted on the OMEGA laser to test this new spectrometer. The targets used were 15 μm thick CH shells with a diameter of 865 μm, filled with 15 atm of approximately equimolar DT gas. The targets were driven using 60 laser beams at 351 nm wavelength, with a 1 ns square laser pulse, 25.4 kJ average energy, and SSD,[34] DPR,[35] and SG4 DPP[36] smoothing techniques. These targets are commonly used for diagnostic development, and typically produce (2−3) × 10^{13} DT-n and ion temperatures ∼6 keV. Both types of WRF (Al and NB) and the two foil thicknesses (103 and 162 μm) were used in these first tests. Sample data for shot 70740 using a Al WRF and a 103 μm foil are shown in Fig. 6. The data are shown with error bars. The modeled neutron spectrum (red, Gaussian in shape) is convolved with the IRF to produce a modeled proton spectrum (blue). The inferred neutron yield is Y_n = (3.4 ± 0.4) × 10^{13}, the neutron energy is E_n = 14.05 ± 0.06_{ran} ± 0.05_{sys} MeV, and the width of the neutron spectrum is σ_n = 0.19 ± 0.06 MeV.

As a first fidelity test, these data were compared to the yield measured by the standard suite of nTOF detectors on OMEGA. This comparison, which is shown in Fig. 7 for all eight shots, indicates an excellent agreement between the two measurements. On one shot (70736) the yield was low compared to the typical (2−3) × 10^{13}. The good agreement with the nTOF system demonstrates that the first-principles IRF calculations described in Sec. III accurately capture the scattering dynamics well in the foil and recoil proton response.

For the neutron energy, there is no other diagnostic to readily compare to. The measured energies are shown relative to the mean for each WRF spectrometer in Fig. 8 for the Al (red) and NB (blue) WRFs, and for each foil thickness: 162 μm at left, and 103 μm at right. The error bars shown are random only. The systematic uncertainties primarily due to the WRF calibration using the accelerator technique[31] are

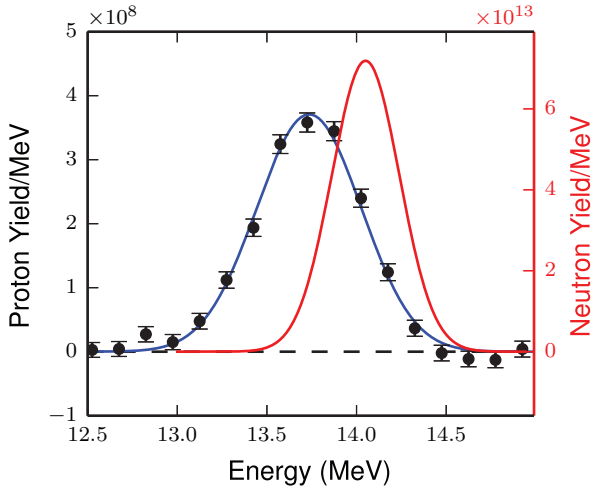

FIG. 6. Forward fit analysis of shot 70740, using a Al WRF and 103 μm foil. The modeled neutron spectrum (red) is convolved with the IRF and adjusted to generate the best fit modeled proton spectrum (blue). The reduced χ^2 for the fit is 0.98.

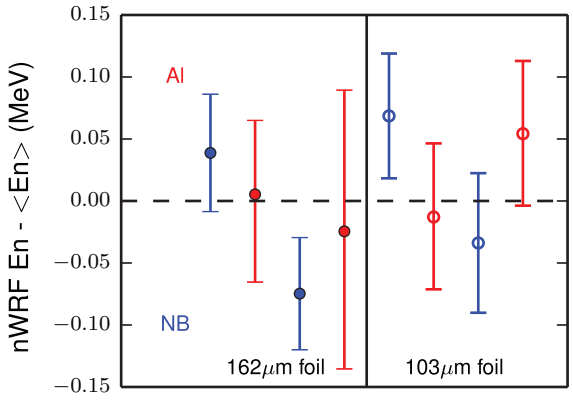

FIG. 8. Mean neutron energies measured with the nWRF spectrometer for all eight shots, relative to the mean for each WRF spectrometer measurement. Shots using the 162 μm foil are shown to the left, and shots with the 103 μm foil are shown to the right. The Al WRF data are shown in red, and the NB data in blue.

too large for the applications of this diagnostic, and we therefore calibrate the system *in situ* using symmetrically driven low-convergence implosions.

V. APPLICATIONS

The primary application for this diagnostic is to measure the mean neutron energy precisely in several directions to infer the bulk velocity of the DT fuel. For this measurement, the uncertainties in mean energy must be reduced. For example, a velocity measurement to a precision of ±50 km/s would require an uncertainty in neutron energy of about ±30 keV (see Fig. 1).

As mentioned in Sec. IV, systematic calibration uncertainties will be eliminated by shooting symmetric low-velocity implosions as a reference, and then shoot implosions of interest or implosions with seeded asymmetries and measure their relative velocity. This would eliminate systematic uncertainties. Another option being pursued is using a DT-n source[37] to calibrate the entire system to a much better precision than can be done currently.

The overall random error bars are ∼±50 keV for this dataset, which is a result of a combination of fitting uncertainties and uncertainties in the WRF analysis (see Appendix A). With improved WRF detectors we expect to reduce this uncertainty to ±30−40 keV on a per-shot basis. This still corresponds to a fairly large velocity of ±50−75 km/s. Since these uncertainties are normally distributed, a series of several shots could be conducted at identical conditions to reduce the energy (velocity) uncertainty to approximately 15−20 keV (25−38 km/s).

Since the implosion residual velocity vector is generally 3D, at least 3 orthogonal lines of sight are required to determine the residual kinetic energy. On the OMEGA laser facility, this diagnostic is fielded in a TIM, and thus up to six could be fielded around an implosion with good 4π coverage to measure the velocity vector in 3D. On the NIF, the x-ray imaging diagnostics fielded in the diagnostic manipulators (DIMs) could be modified to create a nWRF by replacing the pinhole assembly with a scattering foil, and the kinematic base filter pack with a WRF detector, forming a system with comparable dimensions to the system used on OMEGA in this work. The DIMs are located at target chamber coordinates (polar angle θ, azimuthal angle ϕ) of (0,0), (90,78), and (90,315). Fielded simultaneously in all three DIMs, this system could measure the 3D velocity vector in NIF implosions.

The current nWRF design can operate between $10^{12}-10^{14}$ DT neutron yield on OMEGA, though the data presented in this work span $4 \times 10^{12}-4 \times 10^{13}$ (see Fig. 7). At higher yields, CR-39 track saturation[38] is an issue, which can be mitigated by the use of thinner and/or smaller foils at the cost of the signal to background ratio. At lower yields, signal statistics can become poor, necessitating the use of thicker foils at the cost of poorer energy resolution. On the OMEGA facility, no current measurement of bulk velocity exists, so the implementation of this new diagnostic enables physics studies of residual kinetic energy. However, the instrument is incompatible with the stand-off requirements for cryogenic targets on OMEGA. The primary application on OMEGA is to use this instrument to benchmark implosion physics models by imposing known flux asymmetries on warm targets and accurately measuring the resulting residual kinetic energy.

On the NIF, both the MRS and nTOF neutron spectrometers are currently used to measure DT-n Doppler shifts and infer bulk velocity. The MRS measures bulk velocities to ±30 km/s,[6] and the nTOF detectors measure velocity to ±20 km/s.[39] Therefore on the NIF this technique would not represent an improvement in precision over current techniques, but it would enable verification of existing measurements and a relatively inexpensive expansion of the measurement to new locations: for example, at the north pole where there is no current velocity measurement.

VI. CONCLUSIONS

A compact neutron spectrometer has been developed and implemented on the OMEGA laser facility for measurements of the DT neutron spectrum. A proton spectrometer is used to detect recoil protons from elastic neutron scattering in a CH_2 foil. Monte Carlo simulations are used to characterize the instrument response, which is used in a forward-fitting process of the proton data to infer the incident neutron spectrum. The neutron mean energy is determined to ±50 keV precision, and the neutron yield is determined to ±10%. By placing several recoil spectrometers around an implosion, the mean energy of neutrons emitted in the different directions can be determined and used to study the residual implosion kinetic energy at peak compression in implosions at the OMEGA facility. We also discuss improvements to the system to reduce the uncertainty in mean energy in a single direction to ±15−20 keV.

ACKNOWLEDGMENTS

We thank the operations and engineering staff at OMEGA for supporting these experiments, E. Doeg and R. Frankel for their work processing the CR-39, C. Danly and F. Merrill for the "ride-along" opportunity, and C. Ruiz for helpful discussions.

This work is part of the first author's Ph.D. thesis, and was supported in part by the U.S. DoE (Grant Nos. DE-NA0001857 and DE-FC52-08NA28752), LLNL (Grant No. B597367), LLE (Grant No. 415935- G), the Fusion Science Center at the University of Rochester (Grant No. 524431), and the National Laser Users Facility (Grant No. DE-NA0002035). This material is based upon work supported by the National Science Foundation Graduate Research Fellowship Program under Grant No. 1122374.

APPENDIX A: ERROR ANALYSIS

The measurement uncertainties are mainly due to uncertainties in the proton-spectrometer analysis and uncertainties in the forward fit to the proton spectrum. For shot 70740 (see Fig. 6), the uncertainties in mean proton energy E_p, proton spectral width σ_p, and proton yield Y_p are given in Table I, broken up into random, statistical, and systematic. The random uncertainties are normally distributed shot-to-shot errors, largely resulting from CR-39 response variation,

TABLE I. Proton spectrometer uncertainties for shot 70740.

Quantity	Random uncertainty	Statistical uncertainty	Systematic uncertainty
E_p (MeV)	±0.050	±0.030	±0.050
σ_p (MeV)	±0.026	±0.030	…
Y_p	±6.6%	±10.3%	…

which are separated from the purely statistical (i.e., counting) uncertainties.

The statistical errors are retained as the error bars on the data points in the spectra (i.e., Fig. 6), and thus propagate to an error in the forward fit, which is calculated through a χ^2 analysis of the best fit and thus also include additional uncertainty from the fit itself. The non-statistical random and systematic errors are separately propagated to the total uncertainties in derived neutron quantities. The neutron uncertainties are summarized in Table II.

APPENDIX B: NEUTRON KINEMATICS

The fusion kinematics used in this work follow the relativistic calculations of Ballabio (Ref. 40), which provide small corrections to the standard classical kinematics.[19] In particular, for the mean neutron birth energy E_n and width σ_n we use Eqs. (10) and (17), respectively, of Ref. 40.

The mean neutron birth energy $E_n(T_i)$ is used to calculate the initial velocity: $\gamma_0 = 1 + E_n/(m_n c^2)$ and $v_0 = c\sqrt{1-\gamma_0^{-2}}$. For a given bulk velocity v_b in the detector direction the velocities add relativistically:

$$v' = \frac{v_0 + v_b}{1 + v_0 v_b/c^2}, \quad \gamma' = 1/\sqrt{1-(v'/c)^2}, \tag{B1}$$

with Doppler shifted energy given by

$$E_n' = (\gamma' - 1)m_n c^2, \quad \Delta E_n = E_n' - E_n, \tag{B2}$$

where ΔE_n is the energy shift as plotted in Fig. 1.

For the effect of symmetric radial fuel velocity $\vec{v} = v_r \hat{r}$ with v_r constant, the center of mass of the implosion is not moving but the width of the neutron spectrum will be broadened by the radial velocity. With the detector at $\theta = \phi = 0$ in spherical coordinates, the broadened spectrum is given by

$$Y_n'(E) = \int_0^{\pi} d\theta \sin\theta \int_0^{2\pi} d\phi \frac{1}{\sqrt{2\pi}\sigma_n} e^{-[E - E_n'(v_r \cos\theta)]^2/2\sigma_n^2}, \tag{B3}$$

TABLE II. Neutron uncertainties for shot 70740.

Quantity	Forward fit[a] uncertainty	Random[b] uncertainty	Systematic uncertainty
E_n (MeV)	$^{+0.032}_{-0.030}$	$^{+0.059}_{-0.058}$	±0.053
σ_n (MeV)	$^{+0.044}_{-0.048}$	$^{+0.053}_{-0.056}$	…
Y_n	$^{+9.4}_{-9.1}$%	$^{+11.5}_{-10.9}$%	…

[a]Combination of statistical and fitting uncertainties.
[b]Total random uncertainty, including fitting and statistical contributions.

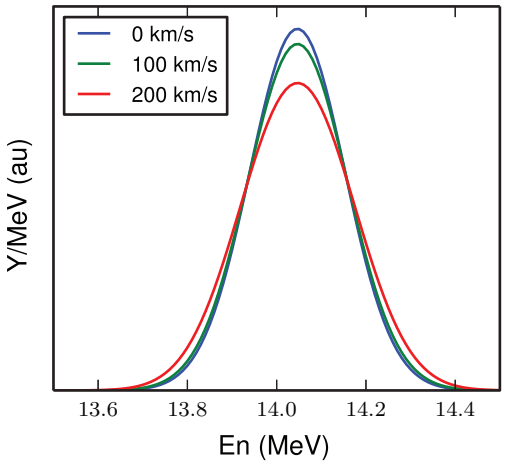

FIG. 9. Neutron spectra for symmetric radial flow velocities of 0, 100, and 200 km/s with $T_i = 5$ keV. Spectra are area normalized.

where for a given location θ, ϕ the neutron spectrum is taken as Gaussian in shape with intrinsic thermal birth width σ_n and shifted energy E_n' using $v_b = v_r \cos\theta$ in the analysis of Eqs. (B1) and (B2). The resulting spectrum $Y_n'(E)$ is evaluated numerically. Example calculations with $v_r = 0$, 100, and 200 km/s are shown in Fig. 9.

From the calculated spectrum with radial flow, a Gaussian width σ_n' is calculated, and the extra width due to the radial flow σ_r is obtained from

$$\sigma_r = \sqrt{\sigma_n'^2 - \sigma_n^2}. \tag{B4}$$

The additional broadening due to radial flow is plotted in Fig. 10.

APPENDIX C: ION TEMPERATURE AND RADIAL VELOCITY

In Appendix B we saw that the width of the neutron spectrum is related to both the ion temperature and any symmetric radial motion of the implosion. The forward-fit analysis (see Sec. IV) calculates the Gaussian width σ with associated

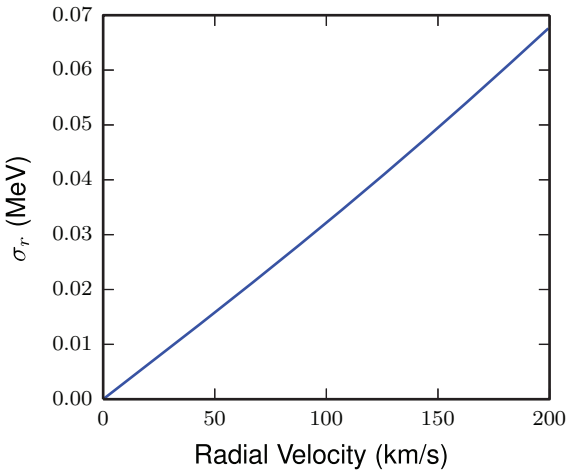

FIG. 10. Extra broadening in the observed neutron spectrum caused by symmetric radial flow.

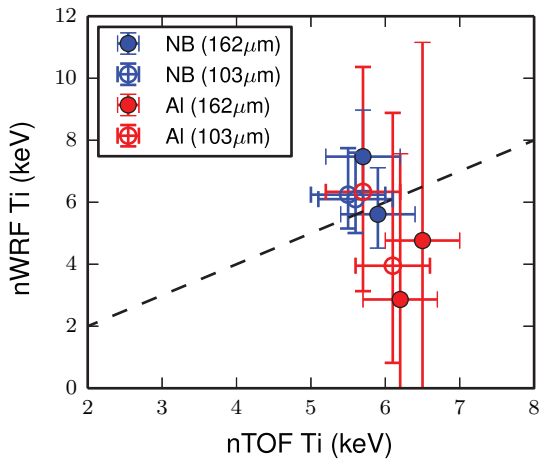

FIG. 11. Ion temperature determined from the nWRF data versus the standard nTOF measurement of T_i.

error bars. If that value is taken directly and used to infer the temperature we obtain the data shown in Fig. 11, which is compared to the nTOF-measured Ti.

The large error bars associated with the nWRF T_i measurements result from the fact that the instrumental response width is larger than the thermal width for these conditions, and uncertainties in the width from the proton spectroscopy and forward fit are amplified since $T_i \propto \sigma^2$. The former is illustrated by Fig. 12, which shows the 1σ widths for the instrument response (~250 keV), the thermal width (in red), and the total width (in blue). The curves are calculated for the 103 μm foil. In this case, the thermal width dominates the instrumental only for $T_i \gtrsim 10$ keV. The NB WRFs perform better than the Al for the temperature determination (demonstrated by smaller error bars in Fig. 11) due to smaller uncertainties in the proton spectroscopy for that design.[20,21]

For thin-glass "exploding pusher" targets on OMEGA, temperatures of 10−20 keV can be achieved, and in this regime the current nWRF configuration would obtain a precise measurement of T_i. Alternatively, thinner foil configurations could be explored to reduce the instrumental width, but at the cost of reduced S/B.

Using the width, symmetric radial flows could similarly be investigated, or differences in ion temperature at various lines of sight around the implosion could be investigated. This would also be a signature of residual kinetic energy. However, we can see in Fig. 10 that the broadening from radial flow is small compared to both the instrumental width and thermal width for these experiments (see Fig. 12). This implies that a measurement of symmetric radial flow velocities would require a significantly reduced instrumental width and implosions with much lower thermal widths, i.e., with $T_i \sim 1-2$ keV.

APPENDIX D: DIRECT NEUTRON BACKGROUND

The primary source of background in this measurement is direct neutron interaction with the WRF or the CR-39 detector; in either case neutrons can undergo (n,p) scattering or other reactions that generate particle tracks in the CR-39 detector, and which must be excluded in the analysis via background subtraction. The S/B is a crucial metric for these sorts of systems, and understanding the background is essential.

Previous work[41] studied the fluence of direct neutron tracks in CR-39 detectors with aluminum filters in front of the CR-39, and the results from that study are directly applicable to the Al WRF data in this work. The background level is shown in Fig. 13 as the fluence of background tracks on the CR-39 versus neutron yield.

As expected there is a clear linear relationship between the neutron yield and background level. Additionally, we show the background level that would be expected from the "frontside" data of Ref. 41, for the 2h CR-39 etch time used in this work, that is $(3 \times 10^{-5})Y_n/(4\pi r^2)$ where $r = 28$ cm is the distance from the implosion to the CR-39 detector. We see excellent agreement between the calibration of Ref. 41 and the observed background levels in this work. We note that the NB WRFs (which are made of alumina) could have a slightly different scaling relation between neutron yield and background level due to different neutron scattering cross-sections, which

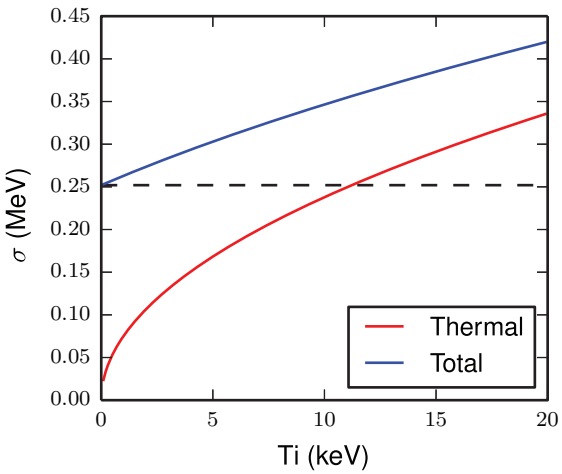

FIG. 12. Broadening (σ) from the instrumental response (dashed line), the thermal width (red), and the total resulting width (blue).

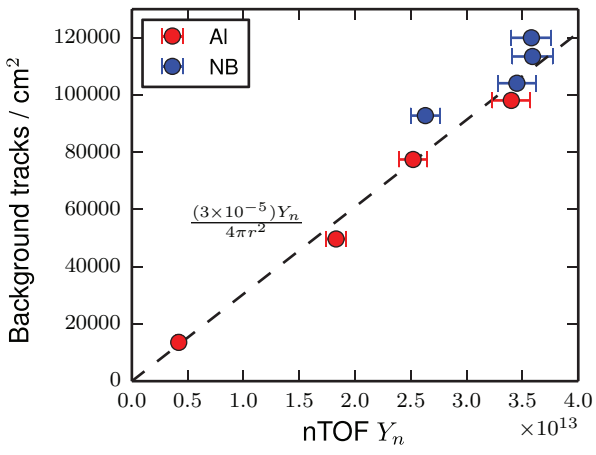

FIG. 13. Measured neutron background versus neutron yield, for the data in this work versus the expected scaling from Ref. 41 (dashed line).

may be observed in Fig. 13. This demonstrates that the background levels are well understood in this type of data.

At high neutron yields, signal and background track densities are high, necessitating short etch times to avoid track overlap.[38]

[1]T. Boehly, D. Brown, R. Craxton, R. Keck, J. Knauer, J. Kelly, T. Kessler, S. Kumpan, S. Loucks, S. Letzring, F. Marshall, R. McCrory, S. Morse, W. Seka, J. Soures, and C. Verdon, Opt. Commun. **133**, 495 (1997).

[2]G. Miller, E. Moses, and C. Wuest, Nucl. Fusion **44**, S228 (2004).

[3]J. Nuckolls, L. Wood, A. Thiessen, and G. Zimmerman, Nature(London) **239**, 139 (1972).

[4]J. Lindl, Phys. Plasmas **2**, 3933 (1995).

[5]S. W. Haan, S. M. Pollaine, J. D. Lindl, L. J. Suter, R. L. Berger, L. V. Powers, W. E. Alley, P. A. Amendt, J. A. Futterman, W. K. Levedahl, M. D. Rosen, D. P. Rowley, R. A. Sacks, A. I. Shestakov, G. L. Strobel, M. Tabak, S. V. Weber, G. B. Zimmerman, W. J. Krauser, D. C. Wilson, S. V. Coggeshall, D. B. Harris, N. M. Hoffman, and B. H. Wilde, Phys. Plasmas **2**, 2480 (1995).

[6]M. Gatu Johnson, D. T. Casey, J. A. Frenje, C.-K. Li, F. H. Sguin, R. D. Petrasso, R. Ashabranner, R. Bionta, S. LePape, M. McKernan, A. Mackinnon, J. D. Kilkenny, J. Knauer, and T. C. Sangster, Phys. Plasmas **20**, 042707 (2013).

[7]J. Kilkenny *et al.*, "Understanding the stagnation and burn of implosions on NIF," EPJ Web Conf. (submitted).

[8]M. Gatu Johnson, J. A. Frenje, D. T. Casey, C. K. Li, F. H. Sguin, R. Petrasso, R. Ashabranner, R. M. Bionta, D. L. Bleuel, E. J. Bond, J. A. Caggiano, A. Carpenter, C. J. Cerjan, T. J. Clancy, T. Doeppner, M. J. Eckart, M. J. Edwards, S. Friedrich, S. H. Glenzer, S. W. Haan, E. P. Hartouni, R. Hatarik, S. P. Hatchett, O. S. Jones, G. Kyrala, S. Le Pape, R. A. Lerche, O. L. Landen, T. Ma, A. J. MacKinnon, M. A. McKernan, M. J. Moran, E. Moses, D. H. Munro, J. McNaney, H. S. Park, J. Ralph, B. Remington, J. R. Rygg, S. M. Sepke, V. Smalyuk, B. Spears, P. T. Springer, C. B. Yeamans, M. Farrell, D. Jasion, J. D. Kilkenny, A. Nikroo, R. Paguio, J. P. Knauer, V. Yu Glebov, T. C. Sangster, R. Betti, C. Stoeckl, J. Magoon, M. J. Shoup, G. P. Grim, J. Kline, G. L. Morgan, T. J. Murphy, R. J. Leeper, C. L. Ruiz, G. W. Cooper, and A. J. Nelson, Rev. Sci. Instrum. **83**, 10D308 (2012).

[9]V. Y. Glebov, D. D. Meyerhofer, T. C. Sangster, C. Stoeckl, S. Roberts, C. A. Barrera, J. R. Celeste, C. J. Cerjan, L. S. Dauffy, D. C. Eder, R. L. Griffith, S. W. Haan, B. A. Hammel, S. P. Hatchett, N. Izumi, J. R. Kimbrough, J. A. Koch, O. L. Landen, R. A. Lerche, B. J. MacGowan, M. J. Moran, E. W. Ng, T. W. Phillips, P. M. Song, R. Tommasini, B. K. Young, S. E. Caldwell, G. P. Grim, S. C. Evans, J. M. Mack, T. J. Sedillo, M. D. Wilke, D. C. Wilson, C. S. Young, D. Casey, J. A. Frenje, C. K. Li, R. D. Petrasso, F. H. Séguin, J. L. Bourgade, L. Disdier, M. Houry, I. Lantuejoul, O. Landoas, G. A. Chandler, G. W. Cooper, R. J. Leeper, R. E. Olson, C. L. Ruiz, M. A. Sweeney, S. P. Padalino, C. Horsfield, and B. A. Davis, Rev. Sci. Instrum. **77**, 10E715 (2006).

[10]C. J. Forrest, P. B. Radha, V. Y. Glebov, V. N. Goncharov, J. P. Knauer, A. Pruyne, M. Romanofsky, T. C. Sangster, M. J. Shoup, C. Stoeckl, D. T. Casey, M. Gatu-Johnson, and S. Gardner, Rev. Sci. Instrum. **83**, 10D919 (2012).

[11]D. L. Bleuel, C. B. Yeamans, L. A. Bernstein, R. M. Bionta, J. A. Caggiano, D. T. Casey, G. W. Cooper, O. B. Drury, J. A. Frenje, C. A. Hagmann, R. Hatarik, J. P. Knauer, M. G. Johnson, K. M. Knittel, R. J. Leeper, J. M. McNaney, M. Moran, C. L. Ruiz, and D. H. G. Schneider, Rev. Sci. Instrum. **83**, 10D313 (2012).

[12]C. B. Yeamans, D. L. Bleuel, and L. A. Bernstein, Rev. Sci. Instrum. **83**, 10D315 (2012).

[13]J. A. Frenje, D. T. Casey, C. K. Li, J. R. Rygg, F. H. Séguin, R. D. Petrasso, V. Yu Glebov, D. D. Meyerhofer, T. C. Sangster, S. Hatchett, S. Haan, C. Cerjan, O. Landen, M. Moran, P. Song, D. C. Wilson, and R. J. Leeper, Rev. Sci. Instrum. **79**, 10E502 (2008).

[14]J. A. Frenje, D. T. Casey, C. K. Li, F. H. Séguin, R. D. Petrasso, V. Y. Glebov, P. B. Radha, T. C. Sangster, D. D. Meyerhofer, S. P. Hatchett, S. W. Haan, C. J. Cerjan, O. L. Landen, K. A. Fletcher, and R. J. Leeper, Phys. Plasmas **17**, 056311 (2010).

[15]D. T. Casey, *Diagnosing Inertial Confinement Fusion Implosions at OMEGA and the NIF Using Novel Neutron Spectrometry* (Massachusetts Institute of Technology, 2012).

[16]D. T. Casey, J. A. Frenje, M. Gatu Johnson, F. H. Séguin, C. K. Li, R. D. Petrasso, V. Y. Glebov, J. Katz, J. P. Knauer, D. D. Meyerhofer, T. C. Sangster, R. M. Bionta, D. L. Bleuel, T. Dppner, S. Glenzer, E. Hartouni, S. P. Hatchett, S. Le Pape, T. Ma, A. MacKinnon, M. A. Mckernan, M. Moran, E. Moses, H.-S. Park, J. Ralph, B. A. Remington, V. Smalyuk, C. B. Yeamans, J. Kline, G. Kyrala, G. A. Chandler, R. J. Leeper, C. L. Ruiz, G. W. Cooper, A. J. Nelson, K. Fletcher, J. Kilkenny, M. Farrell, D. Jasion, and R. Paguio, Rev. Sci. Instrum. **83**, 10D912 (2012).

[17]D. T. Casey, J. A. Frenje, M. Gatu Johnson, F. H. Séguin, C. K. Li, R. D. Petrasso, V. Y. Glebov, J. Katz, J. Magoon, D. D. Meyerhofer, T. C. Sangster, M. Shoup, J. Ulreich, R. C. Ashabranner, R. M. Bionta, A. C. Carpenter, B. Felker, H. Y. Khater, S. LePape, A. MacKinnon, M. A. McKernan, M. Moran, J. R. Rygg, M. F. Yeoman, R. Zacharias, R. J. Leeper, K. Fletcher, M. Farrell, D. Jasion, J. Kilkenny, and R. Paguio, Rev. Sci. Instrum. **84**, 043506 (2013).

[18]J. Frenje, R. Bionta, E. Bond, J. Caggiano, D. Casey, C. Cerjan, J. Edwards, M. Eckart, D. Fittinghoff, S. Friedrich, V. Glebov, S. Glenzer, G. Grim, S. Haan, R. Hatarik, S. Hatchett, M. G. Johnson, O. Jones, J. Kilkenny, J. Knauer, O. Landen, R. Leeper, S. L. Pape, R. Lerche, C. Li, A. Mackinnon, J. McNaney, F. Merrill, M. Moran, D. Munro, T. Murphy, R. Petrasso, R. Rygg, T. Sangster, F. Séguin, S. Sepke, B. Spears, P. Springer, C. Stoeckl, and D. Wilson, Nucl. Fusion **53**, 043014 (2013).

[19]H. Brysk, Plasma Phys. **15**, 611 (1973).

[20]F. H. Séguin, J. A. Frenje, C. K. Li, D. G. Hicks, S. Kurebayashi, J. R. Rygg, B.-E. Schwartz, R. D. Petrasso, S. Roberts, J. M. Soures, D. D. Meyerhofer, T. C. Sangster, J. P. Knauer, C. Sorce, V. Y. Glebov, C. Stoeckl, T. W. Phillips, R. J. Leeper, K. Fletcher, and S. Padalino, Rev. Sci. Instrum. **74**, 975 (2003).

[21]F. H. Séguin, N. Sinenian, M. Rosenberg, A. Zylstra, M. J.-E. Manuel, H. Sio, C. Waugh, H. G. Rinderknecht, M. G. Johnson, J. Frenje, C. K. Li, R. Petrasso, T. C. Sangster, and S. Roberts, Rev. Sci. Instrum. **83**, 10D908 (2012).

[22]D. T. Casey, J. A. Frenje, F. H. Séguin, C. K. Li, M. J. Rosenberg, H. Rinderknecht, M. J.-E. Manuel, M. Gatu Johnson, J. C. Schaeffer, R. Frankel, N. Sinenian, R. A. Childs, R. D. Petrasso, V. Y. Glebov, T. C. Sangster, M. Burke, and S. Roberts, Rev. Sci. Instrum. **82**, 073502 (2011).

[23]G. Morgan, D. Olsen, and J. McConnell, Nucl. Instrum. Methods **157**, 525 (1978).

[24]N. P. Hawkes, P. van Belle, D. S. Bond, S. Croft, and O. N. Jarvis, Rev. Sci. Instrum. **70**, 1134 (1999).

[25]M. J. Moran, V. Y. Glebov, C. Stoeckl, R. Rygg, and B.-E. Schwartz, Rev. Sci. Instrum. **76**, 023506 (2005).

[26]S. W. Conroy, M. Weiszflog, E. Andersson-Sunden, G. Ericsson, M. Gatu-Johnson, C. Hellesen, E. Ronchi, and H. Sjostrand, Rev. Sci. Instrum. **79**, 10E508 (2008).

[27]J. Ziegler, J. Biersack, and U. Littmark, *The Stopping and Range of Ions in Matter* (Pergamon, New York, 1985).

[28]A. Fews and D. L. Henshaw, Nucl. Instrum. Methods Phys. Res. **197**, 517 (1982).

[29]A. P. Fews and D. L. Henshaw, Nucl. Instrum. Methods Phys. Res. **223**, 609 (1984).

[30]N. Sinenian, M. J. Rosenberg, M. Manuel, S. C. McDuffee, D. T. Casey, A. B. Zylstra, H. G. Rinderknecht, M. Gatu Johnson, F. H. Séguin, J. A. Frenje, C. K. Li, and R. D. Petrasso, Rev. Sci. Instrum. **82**, 103303 (2011).

[31]N. Sinenian, M. J.-E. Manuel, A. B. Zylstra, M. Rosenberg, C. J. Waugh, H. G. Rinderknecht, D. T. Casey, H. Sio, J. K. Ruszczynski, L. Zhou, M. G. Johnson, J. A. Frenje, F. H. Séguin, C. K. Li, R. D. Petrasso, C. L. Ruiz, and R. J. Leeper, Rev. Sci. Instrum. **83**, 043502 (2012).

[32]J. A. Frenje, K. M. Green, D. G. Hicks, C. K. Li, F. H. Sguin, R. D. Petrasso, T. C. Sangster, T. W. Phillips, V. Y. Glebov, D. D. Meyerhofer, S. Roberts, J. M. Soures, C. Stoeckl, K. Fletcher, S. Padalino, and R. J. Leeper, Rev. Sci. Instrum. **72**, 854 (2001).

[33]A 4π equivalent yield being the local value of fluence/steradian multiplied by 4π. This is convenient for forward-fitting the WRF analysis, which implicitly assumes isotropic emission.

[34]S. Skupsky, R. W. Short, T. Kessler, R. S. Craxton, S. Letzring, and J. M. Soures, J. Appl. Phys. **66**, 3456 (1989).

[35]D. D. Meyerhofer, J. A. Delettrez, R. Epstein, V. Y. Glebov, V. N. Goncharov, R. L. Keck, R. L. McCrory, P. W. McKenty, F. J. Marshall, P. B. Radha, S. P. Regan, S. Roberts, W. Seka, S. Skupsky, V. A. Smalyuk, C. Sorce, C. Stoeckl, J. M. Soures, R. P. J. Town, B. Yaakobi, J. D. Zuegel, J. Frenje, C. K. Li, R. D. Petrasso, F. H. Sguin, K. Fletcher, S. Padalino, C. Freeman, N. Izumi, R. Lerche, T. W. Phillips, and T. C. Sangster, Phys. Plasmas **8**, 2251 (2001).

[36]Y. Lin, G. N. Lawrence, and T. J. Kessler, Opt. Lett. **21**, 1703 (1996).
[37]C. L. Ruiz, G. A. Chandler, G. W. Cooper, D. L. Fehl, K. D. Hahn, R. J. Leeper, B. R. McWatters, A. J. Nelson, R. M. Smelser, C. S. Snow, and J. A. Torres, Rev. Sci. Instrum. **83**, 10D913 (2012).
[38]A. Zylstra, J. Frenje, F. Sguin, M. G. Johnson, D. Casey, M. Rosenberg, C. Waugh, N. Sinenian, M.-E. Manuel, C. Li, R. Petrasso, Y. Kim, and H. Herrmann, Nucl. Instrum. Methods Phys. Res., Sect. A **681**, 84 (2012).
[39]R. Hatarik, private communication.
[40]L. Ballabio, J. Källne, and G. Gorini, Nucl. Fusion **38**, 1723 (1998).
[41]J. A. Frenje, C. K. Li, F. H. Sguin, D. G. Hicks, S. Kurebayashi, R. D. Petrasso, S. Roberts, V. Y. Glebov, D. D. Meyerhofer, T. C. Sangster, J. M. Soures, C. Stoeckl, C. Chiritescu, G. J. Schmid, and R. A. Lerche, Rev. Sci. Instrum. **73**, 2597 (2002).
[42]F. H. Séguin, M. Gatu Johnson, N. Sinenian, H. Sio, A. Zylstra, M. Manuel, D. Casey, H. Rinderknecht, M. Rosenberg, J. Frenje, C. K. Li, R. D. Petrasso, V. Glebov, J. Knauer, D. D. Meyerhofer, T. C. Sangster, C. Stoeckl, R. Bionta, D. Bleuel, S. Hatchett, A. Mackinnon, D. Munro, O. Landen, C. Yeamans, J. D. Kilkenny, R. J. Leeper, Bull. Am. Phys. Soc. **57**(12), 345 (2012).